



Performance of Dye-Sensitized Solar Cell Using Size-Controlled Synthesis of TiO₂ Nanostructure

A. Talib^{1,2*}, M.K. Ahmad^{1,2}, N. Ahmad^{1,2}, N. Nafarizal^{1,2}, F. Mohamad^{1,2}, C.F. Soon^{1,2}, A.B Suriani³, M.H. Mamat⁴, K. Murakami⁵, M. Shimomura⁵

¹Department of Electronic Engineering, Faculty of Electrical & Electronic
Universiti Tun Hussein Onn Malaysia, 86400, Parit Raja, Batu Pahat, Johor, MALAYSIA

²Microelectronics and Nanotechnology Shamsuddin Research Centre (MiNT-SRC),
Universiti Tun Hussein Onn Malaysia, 86400, Parit Raja, Batu Pahat, Johor, MALAYSIA

³Nanotechnology Research Centre, Department of Physic, Faculty of Science and Mathematics,
Universiti Pendidikan Sultan Idris, 35900 Tanjung Malim, Perak, MALAYSIA

⁴Nano-Electronic Centre, Faculty of Electrical Engineering,
Universiti Teknologi Mara, 40450 Shah Alam, Selangor, MALAYSIA

⁵Department of Engineering, Graduate School of Integrated Science and Technology,
Shizuoka University, 432-8011 Hamamatsu, Shizuoka, JAPAN

*Corresponding Author

DOI: <https://doi.org/10.30880/ijie.2020.12.02.013>

Received 29 December 2019; Accepted 27 January 2020; Available online 28 February 2020

Abstract: Titanium dioxide (TiO₂) or titania shows a great interest in solar cell application due to its morphology and crystalline structure. Moreover, it is an affordable compound that could make solar cells more cost economical than traditional silicon solar cells. In this study, one-step hydrothermal method is demonstrated to synthesis rutile TiO₂ nanorods and nanoflowers morphology in nanoscale dimension on different hydrothermal reaction times for Dye-sensitized solar cells application. Increasing the reaction time could influence in formation of higher crystalline rutile phase titania nanostructure before abruptly decreases as the prolong hydrothermal process carry out. The length of the nanorods produced shows increasing behaviour and the growth of nanoflowers are become denser obviously. Band gap estimation is 2.75 eV slightly lower than bulk rutile TiO₂. It shows that the growth mechanism under different reaction times has great influences on the morphologies and alignment of the nanostructure. Further, the DSSCs fabricated using 15 hours reaction time exhibited the best photovoltaic performance with highest efficiency of 3.42% and highest short-circuit photocurrent of 0.7097V.

Keywords: titanium dioxide, hydrothermal, TiO₂, nanorods/nanoflowers, reaction time, DSSCs

1. Introduction

Titanium dioxide (TiO₂) exists in three major types in our nature that is rutile, anatase and brookite. Each polymorph has a unique phase structure known as tetragonal crystalline phase owned by anatase and rutile, whereas orthorhombic phase is belonging to brookite. Every phase of TiO₂ possesses various band gap which is 3.0eV (rutile), 3.2 eV (anatase) and 3.3 eV (brookite) (Khaki *et al.*, 2017). Rutile is well-known as the most steady phase compared to anatase and

*Corresponding author: akhairul@uthm.edu.my

2020 UTHM Publisher. All rights reserved.

penerbit.uthm.edu.my/ojs/index.php/ijie

brookite at high temperatures, which are meta-stable at all temperatures (Mathpal *et al.*, 2013). TiO₂ can be used as photocatalyst (Addamo *et al.*, 2008; Venkatachalam *et al.*, 2007), water splitting, superhydrophilicity in self-cleaning glass and anti-fogging coating (Huang *et al.*, 2017), removing airborne pollutants and wastewater treatment (Tayade *et al.*, 2007), gas sensors (Radeva *et al.*, 2006), Li-ion batteries materials (Yang *et al.*, 2012), and conversion solar energy to the electricity development (Zhao *et al.*, 2007; Kontos *et al.*, 2008).

The morphology of TiO₂ is an important feature in many uses because there are a lot of main chemical and physical occasions occur on the surface. Accordingly, substantial numbers of researches are presently fixated on the manageable synthesis of TiO₂ with diverse morphologies and different sizes of particle. To date, a variety of preparation procedures have been established for the synthesis of TiO₂, such as sol-gel process (Maheswari & Venkatachalam, 2015), template-assisted (Venkatesan & Kannan, 2017), hydrothermal (Ahmad *et al.*, 2016), chemical bath deposition (Dhandayuthapani *et al.*, 2016), spray pyrolysis (Oja *et al.*, 2004) and anodization (Nishanthi *et al.*, 2014; Sennik *et al.*, 2014). Among them, the hydrothermal process is very facile, convenient and controllable method to fabricate TiO₂ in this research.

Basically, DSSCs comprise a photoanode (the widely used TiO₂), dye-molecules (N-719), a photocathode (Platinum), and an electrolyte solution with contains iodide (I), which can generate iodide/triiodide (I⁻/I₃⁻) ion redox pairs during illumination. Recently, lots of researchers have focused their efforts in enhancing the power conversion efficiency (PCE) of DSSCs by manipulating the photoanode with different structures (Low *et al.*, 2018). Hence, many scholars have made endeavors to improve the transportation of electron for the improvement of the photovoltaic performance of DSSCs by controlling the structure and composition of the titania photoanode.

TiO₂ nanostructures have been synthesized via different methods and evaluated. Nanosheet (Lara *et al.*, 2018), nanowall (Daneshvar e Asl *et al.*, 2019), nanorod (Daneshvar e Asl *et al.*, 2019), nano/micro-sphere (Daneshvar e Asl *et al.*, 2019; Zaki *et al.*, 2018), nanotube (Zaki *et al.*, 2018), nanotree (Fang *et al.*, 2017), skeleton structure (Dong *et al.*, 2003), microsponge (Lu *et al.*, 2011), nanoworm (Hou *et al.*, 2014), nanopillar (Gong *et al.*, 2013), leaf-like mesostructure (Deepak *et al.*, 2014), micropetal (Zhang *et al.*, 2016), and nanostar (Pawar *et al.*, 2016) are some examples of these structures (Daneshvar e Asl *et al.*, 2019). It was identified that these nanoparticles can be controlled by the temperature of hydrothermal and the TiO₂ precursor crystallization.

In this paper, one-step hydrothermal method is demonstrated to synthesis TiO₂ nanorods / nanoflowers (NRs / NFs) morphology and the effect of the different reaction time has been studied and discussed. It shows that the growth mechanism under different relatively dependent parameters has significant influences on the morphologies, sizes and alignment of the structure synthesized.

2. Materials and Methods

2.1 Preparation of TiO₂ NRs/NFs

All the chemicals were methodical grade and tested deprived of advance purification. Fluorine doped Tin Oxide (FTO) glass (7Ω/sq) with a thickness of 2.0 mm was cut into the pieces of 1.5 × 2.5 cm in dimension as substrates. These substrates were cleaned ultrasonically in acetone followed by ethanol and eventually deionized (DI) water (18.2MΩ, Mili-Q Ultrapure) for 10 minutes, respectively. In a typical synthesis, 80 mL deionized water and 80 mL concentrated hydrochloric acid (HCl) (36.5%-38.0% by weight) stirring for 5 minutes before a desired amount of TBOT was further lowered down by drop wise by means of using capillary tube and stirring for another 10 minutes.

The solution of mixture was relocated into a 300 ml Teflon-lined stainless-steel autoclave where the FTO substrates were horizontally placed with an active side facing upward. Then the autoclave was sealed completely for hydrothermal synthesis with temperature of 150 degree Celsius (°C) (Ahmad *et al.*, 2016). The experiment was carried out for different reaction times of 5, 10, 15 and 25 hours respectively. After cooling down to ambient temperature, the substrates were extracted out, cleaned comprehensively with deionized water and permitted to dry naturally in room temperature.

2.2 Fabrication of DSSC

For the fabrication of DSSCs efficiency study, the arranged TiO₂ photoanode with 0.25 cm² working area was submerged for about 24 hours in 0.3 mM of N719 dye at room temperature. The Platinum (Pt) counter electrode was arranged by sputtering technique. In order to bring together the DSSC, the electrolyte drop were arranged from 1,2-dimethyl-3-propylimidazolium iodide, 1.59 g, iodolyte AN 50, 10 ml, 4-tert-butylpyridine, 10 ml, guanidine thiocyanate, 0.01 g and valeronitrile, 5 ml was interleaved in between the two electrodes before braced for solar cell measurement (Fazli *et al.*, 2017).

2.3 Characterization Techniques

The structure of crystal of the as-synthesized films was inspected by Bruker D8 Advance X-ray diffraction (XRD) with CuKα radiation (λ) 1.5406 Å in the Bragg angle ranging from 20° to 70° at a skimming speed of 2°min⁻¹ and the type of slot used was secured divergence slit. X-ray tube voltage and current were fixed at 40 kV and 40 mA, respectively. The morphology and microstructure of the samples were inspected by field emission scanning electron microscopy (FE-SEM, JOEL, JSM-7600F). The energy dispersive X-ray (EDX) spectroscopy (Oxford Instruments, X-Max 50 mm2

detector, operating voltage of 10 kV, and working distance of 15.0 mm) piloted to examine the composition analysis and the samples. The samples optical properties were evaluated using ultraviolet-visible (UV-Vis) spectrophotometry (Shimadzu Corporation, UV-1800).The resistivity of the samples was obtained by four-point probe measurement (Keithley 2400), Photovoltaic performances of the contrived DSSCs were analysed by using a computer-programmed Keithley 2420 Source Meter beneath the simulated sunlight illumination (100 mW/cm-2, AM 1.5) and a solar simulator (Oriel, 91160-100091192, Parccell Technologies) was used as a light source. Finally, the incident of photon-to-current conversion efficiency (IPCE) spectra characteristics were analyzed using Peccel PEC-S20 Action Spectrum Measurement System.

3. Results and Discussion

3.1 Structural Properties

XRD patterns of TiO₂ NRs/NFs obtained by hydrothermal method are shown in Fig. 1. It provides the information of crystalline quality and the orientation of the nanostructure.

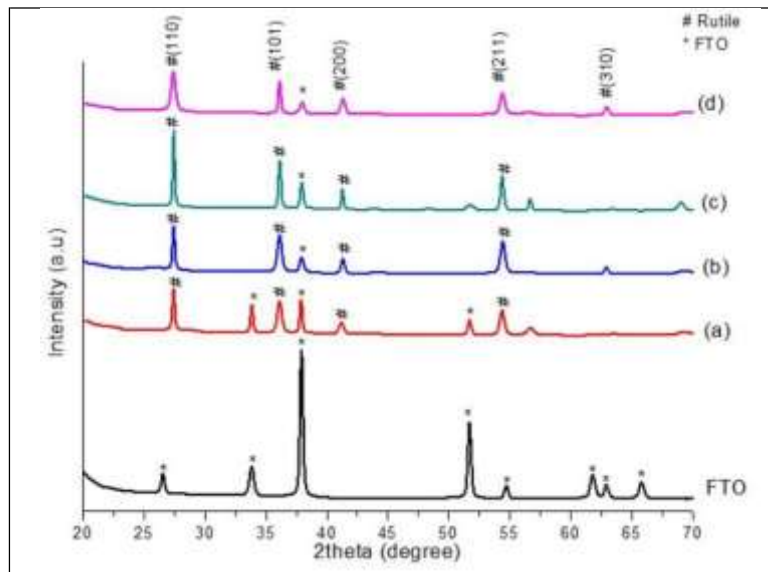


Fig. 1 - XRD patterns of the prepared samples synthesis at (a) 5; (b) 10; (c) 15; and (d) 25 hours

Table 1 - Full-width Half-Maximum and crystallite size of sample fabricated with different reaction time

Reaction time (h)	2θ (°)	Intensity (a.u)	β	Crystallite size, D (nm)	Plane (h k l)
5	27.40	70	0.1968	49.52	110
10	27.42	119	0.1476	69.27	110
15	27.41	135	0.1476	69.27	110
25	27.39	60	0.3936	23.73	110

The nanostructure synthesized displayed the nature of crystalline with diffraction points lying at $2\theta = 27.5^\circ, 37.0^\circ, 41.0^\circ, 54.1^\circ$ and 64.0° can be indexed to (110), (101), (200), (211) and (310) crystal planes. The preferred orientation corresponding to the plane (110) is observed for sample synthesized at 15 hours and identified as sharpest and strongest peak. As the reaction time increase to 25 hours, a broad and lower in intensity peak could be observed suggested to a poor crystallinity of the sample. All the points in the XRD patterns can be assigned well as tetragonal rutile phase of TiO₂ and the diffraction data were in good compliance with JCPDS files no. 21-1276 (Lin *et al.*, 2014). No points corresponding to other phases of TiO₂ such as anatase and brookite or any impurities were detected approving the formation of high purity and stable rutile phase of TiO₂.

Crystallite size was attained by Scherrer’s formula specified by equation (1):

$$D = \frac{K\lambda}{\beta \cos \theta} \tag{1}$$

where D is the crystal size; λ is the wavelength of the X-ray radiation (λ=0.15406 nm) for CuKα; K is constant and regularly reserved as 0.9; and β is the line width at half-maximum height, and θ (theta) is half of the diffraction angle (rad) (Viswanathan & Raj, 2009). The minimum crystallite size attained through this formula is nearly ~50 nm at the first 5 hour and increasing dramatically to ~70 nm in 10 hours reaction time and consistent in the next 15 hours before decreasing abruptly to 23.73 nm at 25 hours, respectively due to maximum peak broadening which in turn indicates its rapid size reduction when the hydrothermal reaction time is take place more than 15 hours as shown in Table 1. This result indicated that crystal structure sizes of the resulting rutile increased with increasing the reaction growth time and consistent for a few hours before the growth is started to decrease as the equilibrium states is achieved for the samples were carried out for more than 15 hours. This result is consistent with the results of the XRD pattern that has been discussed. The crystallite size increases when time increases as increasing time allowing greater coalescence of the particles (Mokhtar *et al.*, 2018).

3.2 Morphological Properties

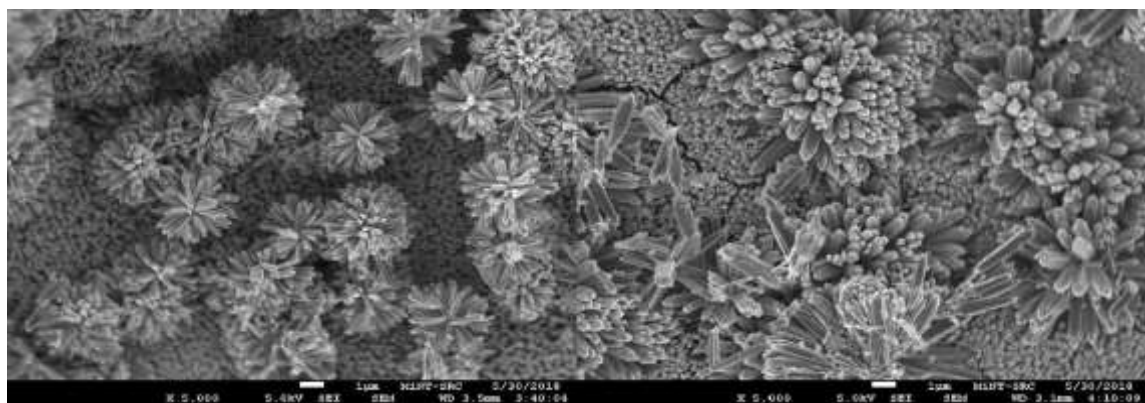
The morphology of nanostructured TiO₂ grown on the FTO and their cross-sectional area were observed using FESEM including the thickness of the structure as shown in Fig. 2. The NRs have grown uniformly and the NFs distributed randomly occupy on several FTO surface. As the time elevated, the growth of both nanostructures becomes increases, more pack and denser and almost occupied the whole of substrate the surface. The size variation of NRs and NFs TiO₂ prepared by manipulating hydrothermal synthesis duration is depicted in Table 2.

Table 2 - The size of TiO₂

Reaction time (h)	Length of nanorods (nm)	Total length (nm)
5	1,650	5,140
10	2,883	9,280
15	3,150	14,950
25	5,720	20,600

Observation under FE-SEM shows images of cross-sectional area are composed of well-align NRs arrays grown on the active surface of FTO substrate decorated by NFs on the top of it under various reaction times ranging from 5 to 25 hour. The nucleation has just begun at more than 3 hours hydrothermal synthesis and 5 hours synthesis is chosen because it is an enough time to growth the double-layered structure (Liu & Aydil, 2009). This double-layered structure combination believes are very beneficial in providing the conductive path for electron and increasing the light scattering for better light harvesting for 1D and 3D layer respectively (Shalini *et al.*, 2018).

The influence of atom arrangement at the conductive side on the substrate and the precursor are significantly affected to the epitaxial and anisotropic nucleation and their growth mechanism (Y. Jiang *et al.*, 2014). FTO active side is consisted of crystal tetragonal structure layer with space group *P4₂/mnm*; JCPDS file no: 77-0452, a=b=0.47538nm, c=0.3186nm while TiO₂ also has a crystalline tetragonal structure belong to space group *P4₂/mnm*; JCPDS No.75-1750, a=b=0.45937nm and c=0.29587nm (Jithin *et al.*, 2017). A similar crystal structure with small lattice mismatch around 2% would favour the epitaxial nucleation and rutile TiO₂ nanostructure growth on FTO substrate (Burungale *et al.*, 2016).



(a)

(b)

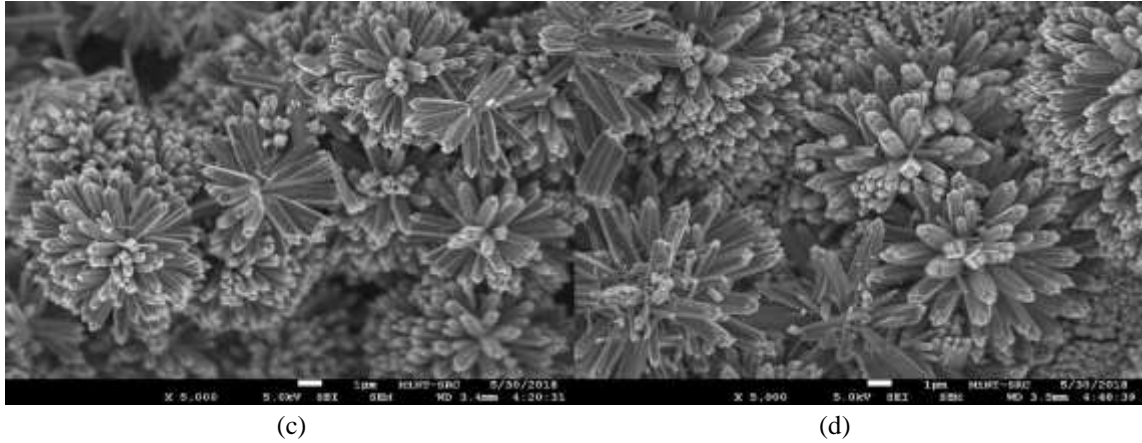


Fig. 2 - FE-SEM images of TiO₂ structure synthesized at different reaction time (a) 5; (b) 10; (c) 15; (d) 25 hours

The EDX analysis has been demonstrated to determine the element composition in each of the sample and simplified in Table 3. Prolonging the synthesis time to 25 hours increased the weight percentage of Ti element composition from 37.06% for 5 hours, 39.44% for 19 hours, 40.80% for 15 hours and 45.50% for 25 hours. While having decreased in the O element composition from 62.94% for 5 hours, 60.34% for 10 hours, 59.20% for 15 hours and 54.60% for 25 hours. Therefore, it can be suggested that Ti element is increased while O element is decreased as the hydrothermal duration took place in prolonged time. These results are in accordance with previous literature related to the synthesis of NRs/NFs TiO₂ structure at various reaction times (Ahmad *et al.*, 2016).

Table 3 - EDX data for samples prepared at different reaction

Reaction time (h)	Element (W = weight% A= atomic%)	
	O	Ti
5	W = 62.94 A = 36.19	W = 37.06 A = 63.81
10	W = 60.34 A = 33.69	W = 39.44 A = 66.31
15	W = 59.20 A = 31.46	W = 40.80 A = 68.54
25	W = 54.60 A = 28.66	W = 45.40 A = 71.34

3.3 Optical Properties

Fig. 3 (a) illustrates the UV-Vis diffuse reflectance spectrum of the NRs/NFs TiO₂ structure. The absorption band edges were expected around 400 nm slightly higher than normally reported of $\lambda = 388$ nm TiO₂. The intercept of the tangent to the plot $(\alpha h\nu)^{1/2}$ versus $(h\nu)$ as depicted in **Figure 3(b)** gives a good approximation of the band gap energy for this indirect band gap material. The graphs show the decreasing behaviour for TiO₂ band gap nanostructures as the reaction time increasing. The band gap energies (E_g) of as-prepared TiO₂ film of 15 hours are around 2.7 eV which are smaller than the value of 3.0 eV for the bulk rutile TiO₂ (Khaki *et al.*, 2017).

The band gap increases with decreasing particle size and the absorption edge is shifted to a higher energy with decreasing particle size. The band gap values validate the crystallite size results according to which smaller crystallite size due to shorter reaction time should have larger band gap and large crystallite size should have smaller band gap when increasing the hydrothermally growth time of nanostructures. However, Jiang *et al.* claimed that the reduced band gap can be attributed to the surface oxygen deficiencies which resulted from the low temperature treatment (N. Jiang *et al.*, 2019).

3.4 Electrical Properties

The current-voltage (I-V) analysis was carried out to measure the electrical properties of the TiO₂ thin film by using four-point probe and the resistivity of the samples were obtained by the equation:

$$R_s = \frac{\rho}{t} \quad (2)$$

where R_s is sheet resistance, ρ is resistivity and t are the thickness of the growth film and the result are depicted in Table 4. The resistivity of the TiO_2 NRs/NFs bi-layer structure is greatly dependent to the thickness of the thin film prepared. The thickness of TiO_2 NRs/NFs increases when hydrothermal process duration carried out in an elongated time thus create the high barrier to the electron simultaneously reduced the conductivity of the samples.

The DSSCs efficiency of the TiO_2 films is identified from the characteristics of photocurrent-voltage displayed in Fig. 4 under a virtual sunlight at 100 mW/cm^2 . The information of the performances of the DSSCs was precised in Table 5 for rutile phased TiO_2 photoanode.

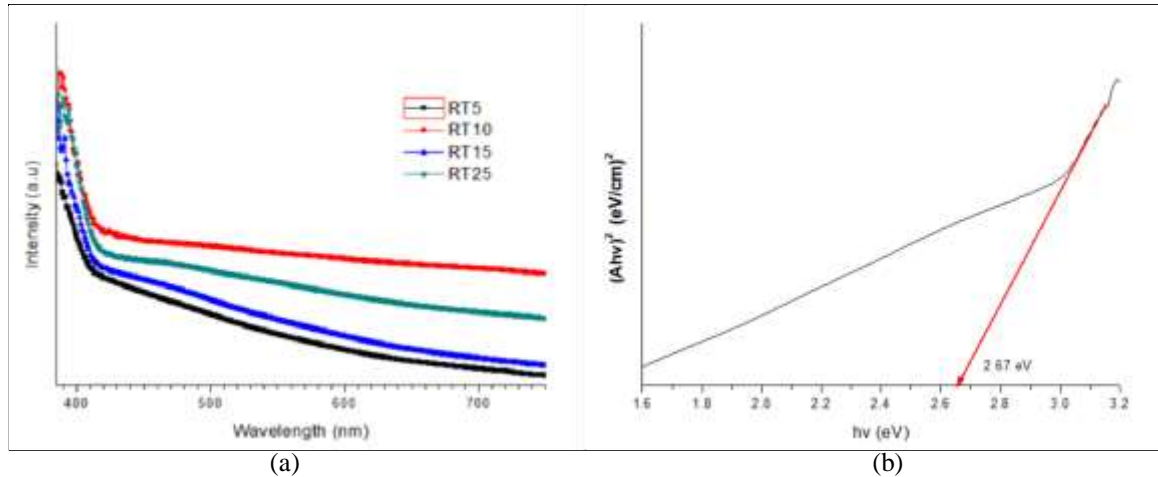


Fig. 3 - (a) UV-Vis absorbance spectrum for 5, 10, 15 and 25 hours; (b) band gap estimation for sample synthesis at 15 hours

Table 4 - Electrical properties of the sample under various reaction

Reaction time (h)	Sheet resistance, R_s ($\times 10^3 \Omega/\text{cm}^2$)	Resistivity, ρ ($\Omega\text{-cm}$)	Thickness of TiO_2 film (μm)
5	4.23	3.98	5.14
10	8.93	8.74	9.28
15	5.05	16.8	14.95
25	3.07	19.7	20.6

Table 5 - Photovoltaic parameters of DSSCs with different TiO_2 reaction time

Reaction time (h)	V_{oc} (V)	J_{sc} (mA/cm^2)	Fill Factor (FF)	Efficiency % (η)
5	0.6891	5.6090	53.79	2.08
10	0.6867	6.3039	58.35	2.53
15	0.7097	8.2310	58.62	3.42
25	0.6915	8.1199	53.17	2.91

The current density (J_{sc}) of the rutile photoanode enlarged with the reaction times along with the conversion efficiency (η). The highest conversion efficiency of 3.42% was given by the sample with 15 hours reaction time. A rise in the current density is the core reason for the growing in DSSCs efficiency. The current generated is identified by the number of photoelectrons from the dye molecules. Higher amount of dye molecules adsorbed onto the TiO_2 obviously will create more photoelectrons.

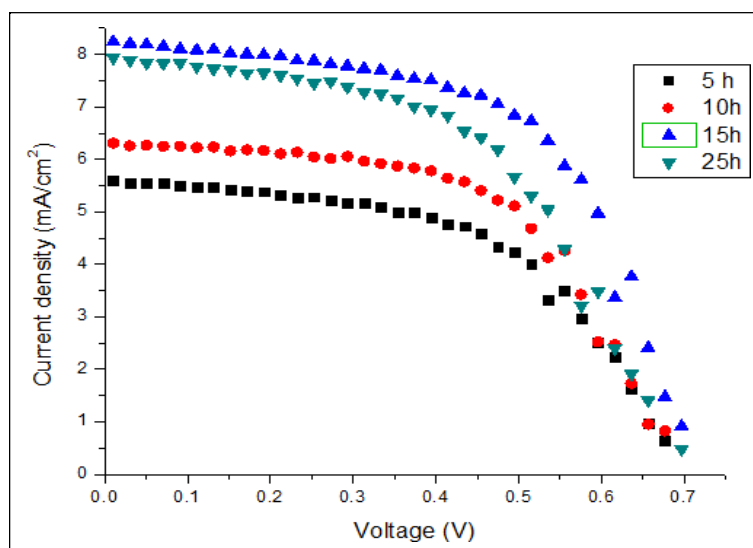


Fig. 4 - J-V characteristics of the DSSCs made with TiO₂ photoanodes of different reaction time

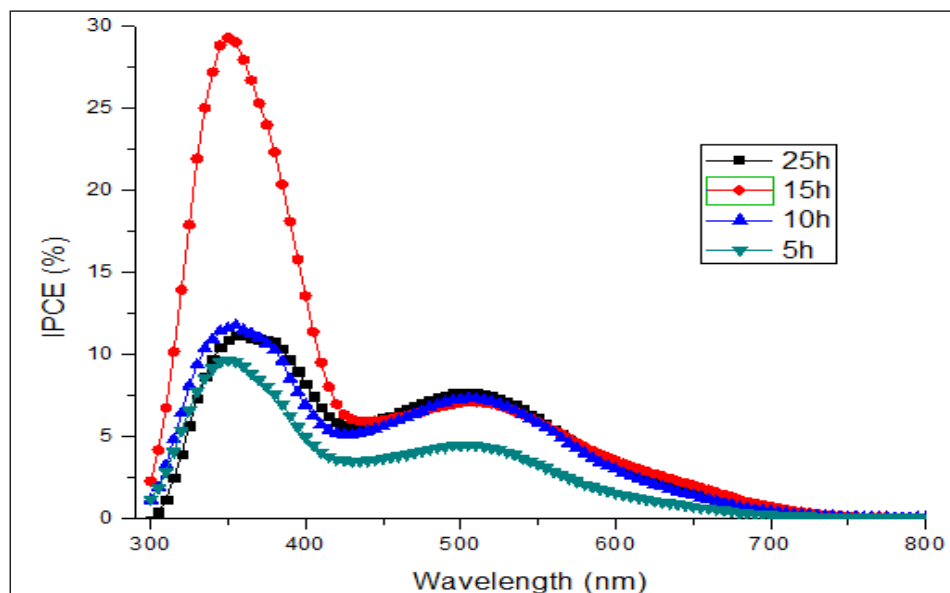


Fig. 5 - The IPCE spectra of DSSCs made with TiO₂ films of different reaction time

The amount of dye molecules adsorbed onto the TiO₂ can be determined by the surface area and the height of the NRs and NFs of the TiO₂ samples. The enhancement of DSSCs efficiency from 2.08% to 3.42% when the TiO₂ hydrothermal reaction times increased is further established by IPCE measurements characterization shown in **Figure 5**. The variation of IPCE values with different TiO₂ reaction times also trails the similar development as the efficiency variation. All the maximum IPCE highest values are in the wavelength array from around 300 to 420 nm. The extreme IPCE peak value of 29.31% parallels to the DSSC with the TiO₂ reaction times of 15 hours. The rise in photon-to-current conversion efficiency up to this specific reaction time is manifestly connected to the rise in injection current from agitated dyes to the conduction band of TiO₂. As the utmost photon-to-current conversion efficiency parallels to the 15 hours reaction time, the maximum rate of photon absorption by the dye and the maximum rate of electron injection from the dye to the conduction band of TiO₂ obviously happen at this optimal point.

4. Conclusion

TiO₂ thin films were successfully synthesized through one-step hydrothermal method on the FTO substrate. The growth of the rod-like structure layer is derived by tetragonal structure with small lattice mismatch. By means of parameters dependent modification, the morphological, sizes and alignment of the structure could be easily controlled. This is confirmed by FESEM images that reveal the presence of the NRs/NFs structure layer that could be tuned by dependent parameters. Band gap estimation is 2.75 eV slightly lower than bulk rutile TiO₂. It shows that the growth mechanism under different reaction times has great influences on the morphologies and alignment of the nanostructure.

Further, the DSSCs fabricated using 15 hours reaction time exhibited the best photovoltaic performance with highest efficiency of 3.42% and highest short-circuit photocurrent of 0.7097 V.

Acknowledgement

This research was supported by Program Hadiah Latihan Persekutuan 2017/2018, funded by Ministry of Higher Education Malaysia, Microelectronic and Nanotechnology - Shamsuddin Research Centre (MiNT-SRC) and Universiti Tun Hussein Onn Malaysia (UTHM) for the facilities and chemicals provided as well the colleagues and expertise from technical support team.

References

- [1] Addamo, M., Augugliaro, V., Di Paola, A., García-López, E., Loddo, V., Marci, G., & Palmisano, L. (2008). Photocatalytic thin films of TiO₂ formed by a sol-gel process using titanium tetraisopropoxide as the precursor. *Thin Solid Films*, 516(12), 3802-3807.
- [2] Ahmad, M. K., Mokhtar, S. M., Soon, C. F., Nafarizal, N., Suriani, A. B., Mohamed, A., ... Murakami, K. (2016). Raman investigation of rutile-phased TiO₂ nanorods/nanoflowers with various reaction times using one step hydrothermal method. *Journal of Materials Science: Materials in Electronics*, 27(8), 7920-7926.
- [3] Ahmad, M. K., Soon, C. F., Nafarizal, N., Suriani, A. B., Mohamed, A., Mamat, M. H., ... Murakami, K. (2016). Effect of heat treatment to the rutile-based dye sensitized solar cell. *Optik*, 127(8), 4076-4079.
- [4] Burungale, V. V., Satale, V. V., More, A. J., Sharma, K. K. K., Kamble, A. S., Kim, J. H., & Patil, P. S. (2016). Studies on effect of temperature on synthesis of hierarchical TiO₂ nanostructures by surfactant free single step hydrothermal route and its photoelectrochemical characterizations. *Journal of Colloid and Interface Science*, 470, 108-116.
- [5] Daneshvar e Asl, S., Eslami Saed, A., & Sadrnezhad, S. K. (2019). Hierarchical rutile/anatase TiO₂ nanorod/nanoflower thin film: Synthesis and characterizations. *Materials Science in Semiconductor Processing*, 93(November 2018), 252-259.
- [6] Deepak, T. G., Anjusree, G. S., Pai, K. R. N., Subash, D., Nair, S. V., & Nair, A. S. (2014). Cabbage leaf-shaped two-dimensional TiO₂ mesostructures for efficient dye-sensitized solar cells. *RSC Adv.*, 4(51), 27084-27090.
- [7] Dhandayuthapani, T., Sivakumar, R., & Ilangovan, R. (2016). Growth of micro flower rutile TiO₂ films by chemical bath deposition technique: Study on the properties of structural, surface morphological, vibrational, optical and compositional. *Surfaces and Interfaces*, 4, 59-68.
- [8] Dong, W., Bongard, H. J., & Marlow, F. (2003). New type of inverse opals: Titania with skeleton structure. *Chemistry of Materials*, 15(2), 568-574.
- [9] Fang, L., Wang, X., Wang, Z., Gong, Z., Jin, L., Li, J., ... Sun, Z. (2017). Heterostructured TiO₂ nanotree arrays with silver quantum dots loading for enhanced photoelectrochemical properties. *Journal of Alloys and Compounds*, 730(5 January 2018), 110-118.
- [10] Fazli, F. I. M., Ahmad, M. K., Soon, C. F., Nafarizal, N., Suriani, A. B., Mohamed, A., ... Murakami, K. (2017). Dye-sensitized solar Cell using pure anatase TiO₂ annealed at different temperatures. *Optik*, 140, 1063-1068.
- [11] Gong, Y. M., He, Y. X., Guo, J., & Zhang, H. (2013). A Concise Route to Fabricate TiO₂ Nanoporous and Nanopillar Films Based on Block Copolymer Self-Assembly. *Advanced Materials Research*, 774-776, 931-934.
- [12] Hou, X., Wang, C., Zhu, W., Wang, X., Li, Y., Wang, J., ... Zhou, F. (2014). Preparation of nitrogen-doped anatase TiO₂ nanoworm / nanotube hierarchical structures and its photocatalytic effect. 29, 29-35.
- [13] Huang, L., Jing, S., Zhuo, O., Meng, X., & Wang, X. (2017). Surface Hydrophilicity and Antifungal Properties of TiO₂ Films Coated on a Co-Cr Substrate. *Hindawi BioMed Research Interntional*, 2017.
- [14] Jiang, N., Du, Y., Liu, S., Du, M., Feng, Y., & Liu, Y. (2019). Facile preparation of flake-like blue TiO₂ nanorod arrays for efficient visible light photocatalyst. *Ceramics International*, (January), 1-7.
- [15] Jiang, Y., Li, M., Song, D., Li, X., & Yu, Y. (2014). A novel 3D structure composed of strings of hierarchical TiO₂spheres formed on TiO₂nanobelts with high photocatalytic properties. *Journal of Solid-State Chemistry*, 211, 90-94.
- [16] Jithin, M., Saravanakumar, K., Ganesan, V., Reddy, V. R., Razad, P. M., Patidar, M. M., ... Mahalakshmi, K. (2017). Growth, mechanism and properties of TiO₂nanorods embedded nanopillar: Evidence of lattice orientation effect. *Superlattices and Microstructures*, 109, 145-153.
- [17] Khaki, M. R. D., Shafeeyan, M. S., Raman, A. A. A., & Daud, W. M. A. W. (2017). Application of doped photocatalysts for organic pollutant degradation - A review. *Journal of Environmental Management*, 198, 78-94.
- [18] Kontos, A. I., Kontos, A. G., Tsoukleris, D. S., Bernard, M. C., Spyrellis, N., & Falaras, P. (2008). Nanostructured TiO₂ films for DSSCS prepared by combining doctor-blade and sol-gel techniques. *Journal of Materials Processing Technology*, 196(1-3), 243-248.

- [19] Lara, M. A., Sayagués, M. J., Navío, J. A., & Hidalgo, M. C. (2018). A facile shape-controlled synthesis of highly photoactive fluorine containing TiO₂ nanosheets with high {001} facet exposure. *Journal of Materials Science*, 53(1), 435-446.
- [20] Lin, J., Heo, Y. U., Nattestad, A., Sun, Z., Wang, L., Kim, J. H., & Dou, S. X. (2014). 3D hierarchical rutile TiO₂ and metal-free organic sensitizer producing dye-sensitized solar cells 8.6% conversion efficiency. *Scientific Reports*, 4, 1-8.
- [21] Liu, B., & Aydil, E. S. (2009). Growth of oriented single-crystalline rutile TiO₂ nanorods on transparent conducting substrates for dye-sensitized solar cells. *Journal of the American Chemical Society*, 131(11), 3985-3990.
- [22] Low, F. W., Lai, C. W., & Hamid, S. B. A. (2018). One-step hydrothermal synthesis of titanium dioxide decorated on reduced graphene oxide for dye-sensitized solar cells application. *International Journal of Nanotechnology*, 15(1/2/3), 78.
- [23] Lu, Y. J., Mei, J., Dong, W. J., Fu, J. L., & Li, C. R. (2011). Synthesis of Silver-Modified Sponge-Like Titanium Dioxide Arrays with Biomimetic Structure and its Enhanced Photocatalytic. *Applied Mechanics and Materials*, 117-119, 824-828.
- [24] Maheswari, D., & Venkatachalam, P. (2015). Enhancing the performance of dye-sensitized solar cells based on organic dye sensitized TiO₂ nanoparticles/nanowires composite photoanodes with ionic liquid electrolyte. *Measurement*, 60, 146-154.
- [25] Mathpal, M. C., Tripathi, A. K., Singh, M. K., Gairola, S. P., Pandey, S. N., & Agarwal, A. (2013). Effect of annealing temperature on Raman spectra of TiO₂ nanoparticles. *Chemical Physics Letters*, 555, 182-186.
- [26] Mokhtar, S. M., Ahmad, M. K., Soon, C. F., Nafarizal, N., Faridah, A. B., Suriani, A. B., ... Murakami, K. (2018). Fabrication and characterization of rutile-phased titanium dioxide (TiO₂) nanorods array with various reaction times using one step hydrothermal method. *Optik*, 154, 510-515.
- [27] Nishanthi, S. T., Iyyapushpam, S., Sundarakannan, B., Subramanian, E., & Pathinettam Padiyan, D. (2014). Inter-relationship between extent of anatase crystalline phase and photocatalytic activity of TiO₂ nanotubes prepared by anodization and annealing method. *Separation and Purification Technology*, 131, 102-107.
- [28] Oja, I., Mere, A., Krunks, M., Solterbeck, C.-H., & Es-Souni, M. (2004). Properties of TiO₂ Films Prepared by the Spray Pyrolysis Method. *Solid State Phenomena*, 99-100, 259-264.
- [29] Pawar, U. T., Pawar, S. A., Jin-Hyeok, K., & Patil, P. S. (2016). Dye sensitized solar cells based on hydrothermally grown TiO₂ nanostars over nanorods. *Ceramics International*.
- [30] Radeva, E. I., Martev, I. N., Dechev, D. A., Ivanov, N., Tsaneva, V. N., & Barber, Z. H. (2006). Sensitivity to humidity of TiO₂ thin films obtained by reactive magnetron sputtering. *Surface and Coatings Technology*, 201(6), 2226-2229.
- [31] Sennik, E., Kilinc, N., & Ozturk, Z. Z. (2014). Electrical and VOC sensing properties of anatase and rutile TiO₂ nanotubes. *Journal of Alloys and Compounds*, 616, 89-96.
- [32] Shalini, S., Prabavathy, N., Balasundaraprabhu, R., Kumar, T. S., Velauthapillai, D., Balraju, P., & Prasanna, S. (2018). Studies on DSSC encompassing flower shaped assembly of Na-doped TiO₂ nanorods sensitized with extract from petals of Kigelia Africana. *Optik*, 155, 334-343.
- [33] Tayade, R. J., Suroliya, P. K., Kulkarni, R. G., & Jasra, R. V. (2007). Photocatalytic degradation of dyes and organic contaminants in water using nanocrystalline anatase and rutile TiO₂. *Science and Technology of Advanced Materials*, 8(6), 455-462.
- [34] Venkatachalam, N., Palanichamy, M., & Murugesan, V. (2007). Sol-gel preparation and characterization of nanosize TiO₂: Its photocatalytic performance. *Materials Chemistry and Physics*, 104(2-3), 454-459.
- [35] Venkatesan, A., & Kannan, E. S. (2017). Highly ordered copper oxide (Cu₂O) nanopillar arrays using template assisted electrodeposition technique and their temperature dependent electrical characteristics. *Current Applied Physics*, 17(5), 806-812.
- [36] Viswanathan, B., & Raj, K. J. A. (2009). Effect of surface area, pore volume and particle size of P25 titania on the phase transformation of anatase to rutile. *Indian Journal of Chemistry - Section A Inorganic, Physical, Theoretical and Analytical Chemistry*, 48(10), 1378-1382.
- [37] Yang, M. C., Lee, Y. Y., Xu, B., Powers, K., & Meng, Y. S. (2012). TiO₂ flakes as anode materials for Li-ion-batteries. *Journal of Power Sources*, 207, 166-172.
- [38] Zaki, A. H., El-Shafey, A., Moatmed, S. M., Abdelhay, R. A., Rashdan, E. F., Saleh, R. M., ... El-dek, S. I. (2018). Morphology transformation from titanate nanotubes to TiO₂ microspheres. *Materials Science in Semiconductor Processing*, 75(September 2017), 10-17.
- [39] Zhang, Y., Foster, C. W., Banks, C. E., Shao, L., Hou, H., Zou, G., ... Ji, X. (2016). Graphene-Rich Wrapped Petal-Like Rutile TiO₂ tuned by Carbon Dots for High-Performance Sodium Storage. *Advanced Materials*, 28(42), 9391-9399.
- [40] Zhao, Y., Li, C., Liu, X., & Gu, F. (2007). Highly enhanced degradation of dye with well-dispersed TiO₂ nanoparticles under visible irradiation. *Journal of Alloys and Compounds*, 440(1-2), 281-286.